Population transfer via a finite temperature state

Wei Huang,[1] Baohua Zhu,[2] Wei Wu,[3] Shan Yin,[1,*] Wentao Zhang,[1,†] and Chu Guo[4,‡]

[1]*Guangxi Key Laboratory of Optoelectronic Information Processing, Guilin University of Electronic Technology, Guilin 541004, China*

[2]*School of Material Science and Engineering, Guilin University of Electronic Technology, Guilin 541004, China*

[3]*Department of Physics, College of Liberal Arts and Sciences, National University of Defense Technology, Changsha 410073, China*

[4]*Key Laboratory of Low-Dimensional Quantum Structures and Quantum Control of Ministry of Education, Department of Physics and Synergetic Innovation Center for Quantum Effects and Applications, Hunan Normal University, Changsha 410081, China*

(Received 19 July 2020; accepted 28 September 2020; published 21 October 2020)

We study quantum population transfer via a common intermediate state initially in thermal equilibrium with a finite temperature T, exhibiting a multilevel stimulated Raman adiabatic passage structure. We consider two situations for the common intermediate state, namely a discrete two-level spin and a bosonic continuum. In both cases we show that the finite temperature strongly affects the efficiency of the population transfer. We also show in the discrete case that strong coupling with the intermediate state, or a longer duration of the controlled pulse, would suppress the effect of finite temperature. In the continuous case, we adapt the thermofield-based chain-mapping matrix product states algorithm to study the time evolution of the system plus the continuum under time-dependent controlled pulses, which shows great potential to be used to solve open quantum system problems in quantum optics.

DOI: 10.1103/PhysRevA.102.043714

I. INTRODUCTION

Stimulated Raman adiabatic passage (STIRAP) is one of the most important technologies to implement complete population transfer from an initial state to a target state via a common intermediate state [1–3]. In the standard implementation of STIRAP, two controlled laser pulses in Gaussian shapes, namely the P pulse and S pulse, are used to couple the initial state and the target state to the intermediate state, respectively. When the two pulses are applied in a counterintuitive order, that is, the S pulse occurs before (but overlapping) the P pulse, complete population transfer could be achieved with negligible excitation of the intermediate state. As a result, this technique is very robust against the noise in the pulses as well as the dissipation in the intermediate state.

Due to the robustness of STIRAP, there are many applications in different quantum systems to achieve complete population transfer from one quantum state to another [4], such as quantum optics [5], ion-trap systems [6], superconducting qubits [7,8], cavity systems [9], and quantum dot systems [10]. Interestingly, the STIRAP technique can be employed not only in quantum systems but also in some specific classical systems, since the equations of motions governing these systems are analogous to the Schrödinger equation. For example, we can employ STIRAP to a waveguide coupler to achieve the complete transfer of intensity of light from an input waveguide to an output waveguide [11]. STIRAP can also be used in a surface plasmon polariton (SPP) coupler excited by light on curved graphene sheets [12], integrated terahertz devices [13], and wireless energy transfer [14].

Since its initial proposition in a standard three-level configuration, the setup of STIRAP has been generalized in various directions, for example, fractional STIRAP [15], bright-state STIRAP [16], straddle STIRAP [17,18], two-state STIRAP [2], and composite-pulse STIRAP [19]. These developments mainly focus on enhancing the robustness of STIRAP, or applying STIRAP in more general scenarios of multiple energy levels.

In this paper, we study the setup of straddle STIRAP where population is transferred from one energy level to another via multiple intermediate-energy levels. It has been shown that complete population transfer could be achieved as long as the couplings between the two energy levels and the intermediate-energy levels satisfy certain conditions [18,20]. In Ref. [21], it was further shown that near-perfect population transfer could also be achieved for a finite-width continuum of intermediate states, and it is robust under moderate dissipation. However, to our best knowledge, most of the STIRAP-related works have assumed that the intermediate-energy levels are initially in unoccupied (vacuum) states. In real applications, a frequently met situation is that the intermediate levels are initially in the thermal equilibrium state, for example, two spins coupled via an optical fiber, or an optical cavity [22] (or chain of cavities) initially in thermal equilibrium. In such cases, the excitations in the intermediate levels may participate in and intertwine with the process, thus destroying the previous physical picture for STIRAP. Here, we fill this gap by directly studying STIRAP-like population transfer via an intermediate thermal state. We mainly focus on two different setups: (1) population

*syin@guet.edu.cn
†zhangwentao@guet.edu.cn
‡guochu604b@gmail.com

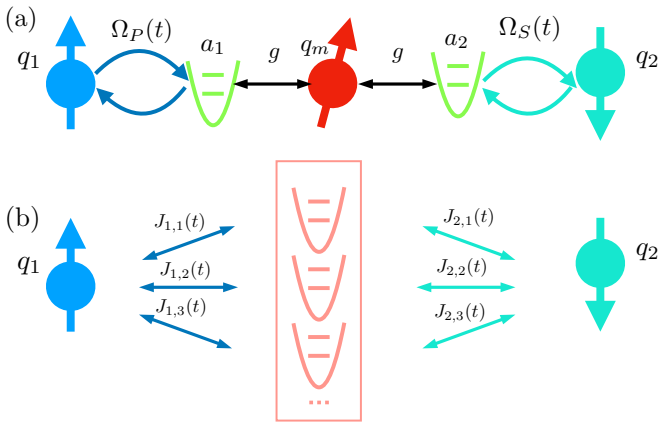

FIG. 1. (a) Population transfer between two qubits q_1 and q_2. The two qubits are coupled to two bosonic modes a_1 and a_2 via two controlled laser pulses $\Omega_P(t)$ and $\Omega_S(t)$, respectively. The two bosonic modes a_1 and a_2 are then coupled to a common intermediate spin q_m with a strength g, which is initially in a thermal state with temperature T. (b) Population transfer between two qubits q_1 and q_2 which couple to a common intermediate bosonic continuum. The bosonic continuum is initially in a thermal distribution with temperature T.

transfer via a discrete two-level system initially in a thermal state with a temperature T and (2) population transfer via a bosonic thermal continuum. We study the effect of a finite temperature intermediate state on the population transfer efficiency by numerically solving the quantum Liouville equation in those setups.

Our paper is organized as follows. In Sec. II, we introduce the discrete version of the model which considers population transfer via a two-level system initially in a thermal state, and show the effect of finite temperature on the efficiency of population transfer. In Sec. III, we introduce the continuous version of the model which considers population transfer via a thermal bosonic continuum and show the effect of finite temperature in this case. We conclude in Sec. IV.

II. DISCRETE INTERMEDIATE STATE

First, we consider population transfer via a discrete thermal state (see Fig. 1). For simplicity, we consider two spins which are coupled to two bosonic modes which act as "flying qubits." The two bosonic modes are then coupled to a common intermediate spin. The Hamiltonian of the whole system can be written as

$$\begin{aligned}\hat{H}(t) = &\frac{\omega_{q,1}}{2}\hat{\sigma}_1^z + \frac{\omega_{q,2}}{2}\hat{\sigma}_2^z + \omega_{a,1}\hat{a}_1^\dagger\hat{a}_1 + \omega_{a,2}\hat{a}_2^\dagger\hat{a}_2 \\ &+ \Omega_P(t)(\hat{a}_1^\dagger\hat{\sigma}_1^- + \hat{a}_1\hat{\sigma}_1^+) + \Omega_S(t)(\hat{a}_2^\dagger\hat{\sigma}_2^- + \hat{a}_2\hat{\sigma}_2^+) \\ &+ \frac{\omega_m}{2}\hat{\sigma}_m^z + g(\hat{a}_1^\dagger\hat{\sigma}_m^- + \hat{a}_1\hat{\sigma}_m^+) + g(\hat{a}_2^\dagger\hat{\sigma}_m^- + \hat{a}_2\hat{\sigma}_m^+),\end{aligned} \tag{1}$$

where $\omega_{q,1}$ and $\omega_{q,2}$ are the energy differences of the two qubits, $\omega_{a,1}$ and $\omega_{a,2}$ are the frequencies of the two bosonic modes, and the time-dependent couplings $\Omega_P(t)$ and $\Omega_S(t)$ between the two qubits and the bosonic mode are induced by two controlled pulses, which are defined as

$$\Omega_P(t) = \Omega \exp\left(\frac{-(t-\tau/2)^2}{\tau_0^2}\right), \tag{2}$$

$$\Omega_S(t) = \Omega \exp\left(\frac{-(t+\tau/2)^2}{\tau_0^2}\right), \tag{3}$$

with τ_0 the standard deviation of Gaussian pulses, τ the time delay between the two pulses, and Ω the maximum strength of the pulses. ω_m is the energy difference of the intermediate spin, and g is the coupling strength between the intermediate spin and the two bosonic modes. We have set $\hbar = 1$. The dynamics of this system is described by the quantum Liouville equation

$$\frac{d\hat{\rho}(t)}{dt} = -i[\hat{H}(t), \hat{\rho}]. \tag{4}$$

In the rest of this work we will always use the resonant condition such that $\omega_{q,1} = \omega_{q,2} = \omega_{a,1} = \omega_{a,2} = \omega_m$. The bosonic modes are not occupied initially while the intermediate spin is assumed to be in a thermal state with a temperature T, that is,

$$\hat{\rho}^m = \frac{1}{1+e^{-\beta\omega_m}}|0^m\rangle\langle 0^m| + \frac{e^{-\beta\omega_m}}{1+e^{-\beta\omega_m}}|1^m\rangle\langle 1^m|. \tag{5}$$

Here, β is the inverse temperature $\beta = 1/T$ and we have set the Boltzmann constant $k_B = 1$. Thus the initial state of the whole system can be written as

$$\hat{\rho}_i = |1^{q_1}\rangle\langle 1^{q_1}| \otimes |0^{a_1}\rangle\langle 0^{a_1}| \otimes \hat{\rho}^m \otimes |0^{a_2}\rangle\langle 0^{a_2}| \otimes |0^{q_2}\rangle\langle 0^{q_2}|, \tag{6}$$

where $|0^{q_i}\rangle$ ($|1^{q_i}\rangle$) means the ground (excited) state of the spin q_i, and $|0^{a_i}\rangle$ means the vacuum state for the bosonic mode a_i, with $i = 1, 2$. The final state after the time evolution is denoted as $\hat{\rho}_f$, namely $\hat{\rho}_f = \hat{\rho}(\infty)$. Moreover, we denote $\mathcal{F}_i(t)$ as the occupation on the excited state of the spin q_i, that is,

$$\mathcal{F}_1(t) = \langle 1^{q_1}|\hat{\rho}^{q_1}(t)|1^{q_1}\rangle, \tag{7}$$

$$\mathcal{F}_2(t) = \langle 1^{q_2}|\hat{\rho}^{q_2}(t)|1^{q_2}\rangle, \tag{8}$$

where $\hat{\rho}^{q_i}(t)$ means the reduced density operator of the spin q_i. In our setup, we have $\mathcal{F}_1(-\infty) = 1$ and $\mathcal{F}_2(-\infty) = 0$, and perfect population is achieved if $\mathcal{F}_1(-\infty) = 0$ and $\mathcal{F}_2(-\infty) = 1$. In the following we will use $\mathcal{F} = \mathcal{F}_2(\infty)$ to denote the final fidelity.

To show the effect of the temperature T and the interplay between T and the other parameters, we simulate the dynamics of Eq. (4) in a wide parameter range, and the results are shown in Fig. 2. In Fig. 2(a), we show the dependence of the final fidelity $\mathcal{F}$ on the temperature T and the coupling strength g between the bosonic modes and the intermediate spin. We can see that $\mathcal{F}$ is greatly suppressed when increasing T, showing that a highly occupied excited state would strongly affect the efficiency of population transfer. We can also see that $\mathcal{F}$ slightly goes up with g, especially at higher temperatures. This is expected since a standard requirement for perfect STIRAP is the strong coupling between the initial (final) states with the intermediate states. This result is

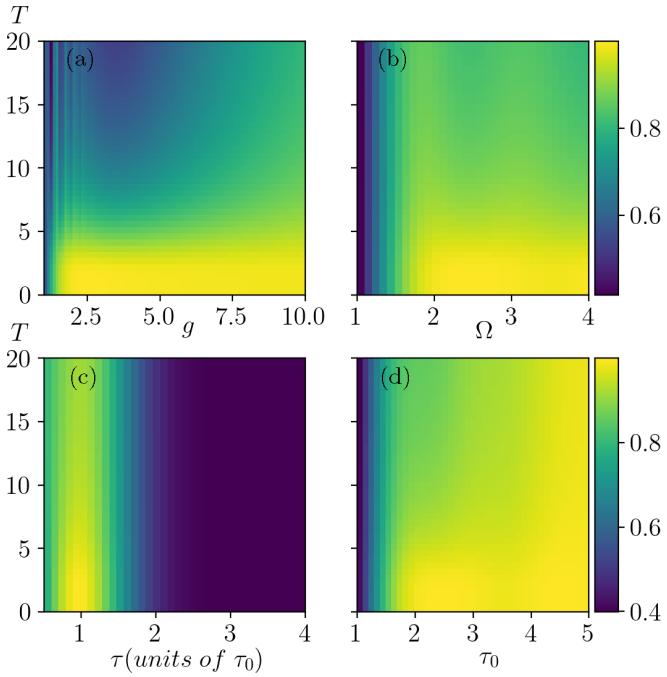

FIG. 2. Dependence of $\mathcal{F}$ on temperature T in the discrete case, where T ranges from 0 to 20 in all panels. (a) $\mathcal{F}$ as a function of g and T, where g ranges from 1 to 10. (b) $\mathcal{F}$ as a function of Ω and T, where Ω ranges from 1 to 4. (c) $\mathcal{F}$ as a function of τ and T, where τ ranges from $0.5\tau_0$ to $4\tau_0$. (d) $\mathcal{F}$ as a function of τ_0 and T, where τ_0 ranges from 1 to 5. The other parameters used in all panels, unless otherwise specified, are $g = 10$, $\Omega = 2$, $\tau = 1$, and $\tau_0 = 2$.

interesting in that it shows that although STIRAP is known to be robust against the dissipation of the intermediate state, however, it will be strongly affected if the intermediate spin is in a highly mixed state. In Fig. 2(b), we show the dependence of $\mathcal{F}$ on T and the maximum amplitude of the laser pulse Ω, with $g = 10$, $\tau = 1$, $\tau_0 = 2$. We can see that the dependence of $\mathcal{F}$ on Ω is similar to the dependence of $\mathcal{F}$ on g. This is because Ω plays a similar role as g which determines the coupling strength between the initial (final) state and the intermediate spin. In Fig. 2(c), we show the dependence of $\mathcal{F}$ on T and the time delay τ. We can see that there is a pick around $\tau = \tau_0$, and since the coupling strength $g = 10$ and $\Omega = 2$ are large enough, a relatively high population transfer efficiency could still be achieved at high temperature. In Fig. 2(d), we show the dependence of $\mathcal{F}$ on T and the period of driving τ_0. We can see that $\mathcal{F}$ is larger with larger τ_0. This is expected since larger τ_0 means the time evolution is slower, thus more adiabatic, which is another standard requirement of STIRAP. For large T, population transfer efficiency is slightly suppressed but much less significant than in the cases shown in Figs. 2(a) and 2(b).

III. CONTINUOUS INTERMEDIATE STATE

Now we further consider the case where two qubits are coupled via an intermediate finite temperature bosonic continuum. The Hamiltonian of the whole system can be written as

$$\begin{aligned}\hat{H}(t) = &\frac{\omega_{q,1}}{2}\hat{\sigma}_1^z + \frac{\omega_{q,2}}{2}\hat{\sigma}_2^z + \int d\omega\omega\hat{b}_\omega^\dagger\hat{b}_\omega \\ &+ \Omega_P(t)\int d\omega\sqrt{\mathcal{J}(\omega)}(\hat{\sigma}_1^+\hat{b}_\omega + \hat{\sigma}_1^-\hat{b}_\omega^\dagger) \\ &+ \Omega_S(t)\int d\omega\sqrt{\mathcal{J}(\omega)}(\hat{\sigma}_2^+\hat{b}_\omega + \hat{\sigma}_2^-\hat{b}_\omega^\dagger),\end{aligned} \tag{9}$$

where $\mathcal{J}(\omega)$ is the spectrum function. We choose a simple subohmic spectrum as

$$\mathcal{J}(\omega) = \sqrt{\omega}, \tag{10}$$

and we also choose a sharp cutoff ω_c such that $\mathcal{J}(\omega) = 0$ for $\omega > \omega_c$, as a signature of a finite-width continuum. In comparison with the discrete case considered in Sec. II, we have removed the two intermediate "flying qubits" a_1 and a_2, which will allow an easier numeric treatment while the resulting physics is still similar. In case the continuum is initially in the zero temperature state, the dynamics of Eq. (9) can be easily solved based on a discretization of the continuum and an exact diagonalization approach since only the single excitation sector needs to be considered [21]. However, for a finite temperature T, the continuum is a mixture of different bosonic particles and the Hilbert space size is in general exponentially large. As a result, exact diagonalization would be impossible in this case. Moreover, in this case a Markovian quantum master equation, such as the Lindblad equation [23,24], would likely be problematic since here we consider strong system-continuum coupling.

In recent years, there is growing interest in using the system-bath approach in combination with the matrix product states method to study the dynamics of open quantum systems. The system and the bath are evolved together as a whole, and the dynamics of the system is obtained by tracing out the bath degrees of freedoms. Here, we use a thermofield-based chain-mapping matrix product states algorithm (TCMPS) [25–31] to study the dynamics of the system plus bath which is the continuum in our case. The main advantage of this method is that the finite temperature bath is mapped into another enlarged bath which is initially at zero temperature, thus favoring a MPS simulation. TCMPS includes three major steps: (1) For the discretization of the bath [32], we use a simple linear discretization scheme with a frequency step size δ, and the discretized Hamiltonian after this step would be

$$\begin{aligned}\hat{H}^{\rm dis}(t) = &\frac{\omega_{q,1}}{2}\hat{\sigma}_1^z + \frac{\omega_{q,2}}{2}\hat{\sigma}_2^z + \sum_{j=1}^{N}\omega_j\hat{b}_j^\dagger\hat{b}_j \\ &+ \Omega_P(t)\sum_{j=1}^{N}J_j(\hat{a}_1\hat{b}_j^\dagger + \hat{a}_1^\dagger\hat{b}_j) \\ &+ \Omega_S(t)\sum_{j=1}^{N}J_j(\hat{a}_2\hat{b}_j^\dagger + \hat{a}_2^\dagger\hat{b}_j),\end{aligned} \tag{11}$$

where we have used $N = \omega_c/\delta$, $\omega_j = j\delta$, $\hat{b}_j = \hat{b}(\omega_j)$, $\hat{b}_j^\dagger = \hat{b}^\dagger(\omega_j)$, $J_j = \sqrt{\mathcal{J}(\omega_j)\delta}$. The time-dependent couplings $J_{1,j}(t)$ and $J_{2,j}(t)$ in Fig. 1(b) correspond to $\Omega_P(t)J_j$ and $\Omega_S(t)J_j$,

respectively. In the limit $N \to \infty$, $\hat{H}^{\rm dis}(t)$ is equivalent to $\hat{H}(t)$ [32,33]. (2) Thermofield transformation maps the bath of N bosonic modes into an enlarged but equivalent bath with $2N$ bosonic modes, and at the same time the thermal state corresponding to the original bath is mapped into the vacuum state of the enlarged bath. The Hamiltonian after this step is

$$\begin{aligned}\hat{H}^{\rm T}(t) = &\frac{\omega_{q,1}}{2}\hat{\sigma}_1^z + \frac{\omega_{q,2}}{2}\hat{\sigma}_2^z + \sum_{j=1}^{N}\omega_j(\hat{c}_{1,j}^\dagger\hat{c}_{1,j} - \hat{c}_{2,j}^\dagger\hat{c}_{2,j}) \\ &+ \Omega_P(t)\sum_{j=1}^{N} g_{1,j}(\hat{a}_1\hat{c}_{1,j}^\dagger + \hat{a}_1^\dagger\hat{c}_{1,j}) \\ &+ \Omega_P(t)\sum_{j=1}^{N} g_{2,j}(\hat{a}_1\hat{c}_{2,j} + \hat{a}_1^\dagger\hat{c}_{2,j}^\dagger) \\ &+ \Omega_S(t)\sum_{j=1}^{N} g_{1,j}(\hat{a}_2\hat{c}_{1,j}^\dagger + \hat{a}_2^\dagger\hat{c}_{1,j}) \\ &+ \Omega_S(t)\sum_{j=1}^{N} g_{2,j}(\hat{a}_2\hat{c}_{2,j} + \hat{a}_2^\dagger\hat{c}_{2,j}^\dagger), \end{aligned} \tag{12}$$

where $g_{1,j} = J_j\cosh(\theta_j)$ and $g_{2,j} = J_j\sinh(\theta_j)$, with $\cosh(\theta_j) = \sqrt{1+n(\omega_j)}$, $\sinh(\theta_j) = \sqrt{n(\omega_j)}$, and $n(\omega) = 1/(e^{\beta\omega}-1)$ to be the Bose-Einstein distribution. (3) The star-to-chain mapping maps the system bath from the star configuration into a chain configuration. The final Hamiltonian after those three steps would be

$$\begin{aligned}\hat{H}^{\rm TC}(t) = &\frac{\omega_{q,1}}{2}\hat{\sigma}_1^z + \frac{\omega_{q,2}}{2}\hat{\sigma}_2^z + \sum_{\nu=1}^{2}\sum_{j=1}^{N_{\rm chain}}\alpha_{\nu,j}\hat{d}_{\nu,j}^\dagger\hat{d}_{\nu,j} \\ &+ \Omega_P(t)\sum_{j=1}^{N_{\rm chain}}(\beta_{1,1}\hat{a}_1\hat{d}_{1,j}^\dagger + \beta_{2,1}\hat{a}_1\hat{d}_{2,j} + {\rm H.c.}) \\ &+ \Omega_S(t)\sum_{j=1}^{N_{\rm chain}}(\beta_{1,1}\hat{a}_2\hat{d}_{1,j}^\dagger + \beta_{2,1}\hat{a}_2\hat{d}_{2,j} + {\rm H.c.}) \\ &+ \sum_{\nu=1}^{2}\sum_{j=1}^{N_{\rm chain}-1}\beta_{\nu,j+1}(\hat{d}_{\nu,j}^\dagger\hat{d}_{\nu,j+1} + {\rm H.c.}), \end{aligned} \tag{13}$$

where $\alpha_{1,j}$ and $\beta_{1,j}$ are the diagonal terms and off-diagonal terms resulting from the Lanczos tridiagonalization of the diagonal matrix diag$([\omega_1, \omega_2, \ldots, \omega_{\rm N}])$ with the initial vector $[g_{1,1}, g_{1,2}, \ldots, g_{1,N}]$, while $\alpha_{2,j}$ and $\beta_{2,j}$ are the diagonal terms and off-diagonal terms resulting from the Lanczos tridiagonalization of the diagonal matrix diag$([-\omega_1, -\omega_2, \ldots, -\omega_{\rm N}])$ with the initial vector $[g_{2,1}, g_{2,2}, \ldots, g_{2,N}]$ [27]. The size of the vectors $\alpha_{2,j}$ and $\beta_{2,j}$, denoted as $N_{\rm chain}$, is usually chosen to be less than N. So we are applying TCMPS to study an open quantum system with time-dependent driving.

We then evolve $\hat{H}^{\rm TC}(t)$ with the same initial state for the two spins as for the discrete case, and a vacuum state for the enlarged continuum corresponding to the set of modes $\hat{d}_{\nu,j}$. In our simulations we have chosen $\omega_c = 2$, $\delta = 0.01$, $N_{\rm chain} = 50$, the truncation of the local Hilbert space size $d = 5$ for each bosonic mode $\hat{d}_{\nu,j}$, a time step size $dt = 0.01$, and we have kept 400 auxiliary states. The largest singular value truncation error observed during the time evolution is of the order 10^{-4}. We have also checked that the difference in the numerical results is negligible when tuning the hyperparameter $N_{\rm chain}$ from 50 to 75, indicating that our results have converged. In Fig. 3(a), we plot $\mathcal{F}_1(t)$ and $\mathcal{F}_2(t)$ as a function of time t; we can see that in the case of $T = 0$, almost perfect population transfer can be achieved, which is also shown in Ref. [21]. As T increases, the efficiency of population transfer goes down significantly. In Fig. 3(b), we plot $\mathcal{F}_1(\infty)$ and $\mathcal{F}_2(\infty)$ as a function of the temperature T, from which we can see more clearly that the efficiently of population transfer goes down significantly when T increases. At $T = 0.5$, we already see that the final fidelity $\mathcal{F} \approx 0.7$, which is likely to further go down as suggested by the trend in Fig. 3(b). However, the simulation for larger T is currently beyond our capacity since a larger truncation d is then required to ensure enough precision. These results show that for STIRAP via an infinite number of intermediate states, the nonzero temperature strongly affects the population transfer efficiency.

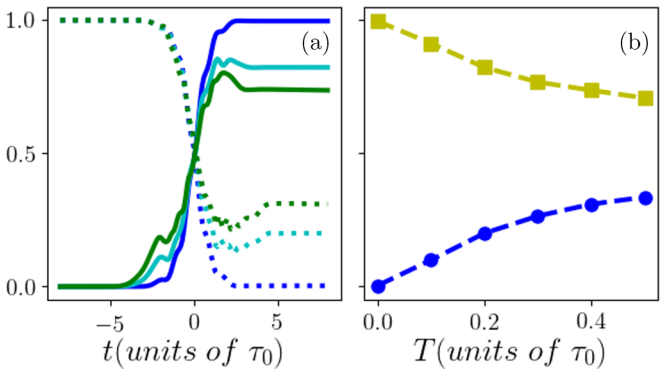

FIG. 3. Population transfer via a thermal bosonic continuum. (a) The solid lines from the top down correspond to $T = 0, 0.2, 0.4$, respectively, which plot $\mathcal{F}_1$ as a function of time t. The dotted lines from the bottom to the top correspond to $T = 0, 0.2, 0.4$, respectively, which plot $\mathcal{F}_2$ as a function of time t. (b) The blue dashed line with circles corresponds to $\mathcal{F}_1(\infty)$ as a function of temperature T, while the yellow dashed line with squares corresponds to $\mathcal{F}_2(\infty)$ as a function of temperature T which ranges from 0 to 0.5.

IV. CONCLUSION

We propose two models to study quantum population transfer between two spins via an intermediate state which is initially in thermal equilibrium. In the first case, we consider a discrete model where the two spins are coupled to two bosonic modes by two controlled pulses $\Omega_P(t)$ and $\Omega_S(t)$ which act as "flying qubits," which are then coupled to a common intermediate spin initially in a thermal state. In the second case, we consider a continuous model where the two spins are directly coupled to a thermal bosonic continuum by the two controlled pulses. In both cases, we show that the efficiency of the population transfer is strongly dependent on the finite temperature of the intermediate state, in contrast with previous results where the population transfer efficiency

is robust against the details of the intermediate states as long as certain control parameters are well tuned.

Moreover, in this work we have adapted the TCMPS method, which is a recently developed numeric technique used to solve open quantum many-body systems, to study quantum population transfer via a thermal bosonic continuum. Our results show that TCMPS could be a perfect numerical tool to study open quantum optics problems in the presence of a finite temperature environment and time-dependent driving.

For possible experimental realizations, we note that similar models have already been realized, for instance, superconducting qubits interacting with an intermediate cavity formed by an open-ended superconducting transmission line [34] as well as Rydberg atoms coupled via a microwave cavity [35]. In the latter case, a cavity frequency of $2\pi \times 5$ GHz in a thermal state with an average occupation $\bar{n} = 10$ has been considered [35]. The only difference between these models and our continuous model is that in these models the cavities are modeled with only a single mode. The continuous case considered in this work naturally follows in the case where the intermediate cavity has to be modeled by a finite range of modes. Additionally, the continuous case could be realized with two spins in solid state systems which are coupled to a phonon environment. The discrete model could be realized, for instance, with atoms coupled to two optical cavities, which are then coupled to a common intermediate atom, immersed in a thermal bath. One could also consider the standard case where the intermediate atom is subjected to both decaying and optical pumping, which is highly tunable and enforces a mixed state (though not exactly a thermal state).

ACKNOWLEDGMENTS

The authors acknowledge funding from the National Science and Technology Major Project (Grant No. 2017ZX02101007-003), National Natural Science Foundation of China (Grants No. 61565004, No. 6166500, and No. 61965005), the Natural Science Foundation of Guangxi Province (Nos. 2017GXNSFBA198116 and 2018GXNSFAA281163), and the Science and Technology Program of Guangxi Province (No. 2018AD19058). W.H. acknowledges funding from the Guangxi overseas 100 talent project and W.Z. acknowledges funding from the Guangxi distinguished expert project. C.G. acknowledges support from National Natural Science Foundation of China under Grant No. 11805279.

[1] N. Vitanov, M. Fleischhauer, B. Shore, and K. Bergmann, Adv. At., Mol., Opt. Phys. **46**, 55 (2001).
[2] N. V. Vitanov, A. A. Rangelov, B. W. Shore, and K. Bergmann, Rev. Mod. Phys. **89**, 015006 (2017).
[3] B. W. Shore, Adv. Opt. Photonics **9**, 563 (2017).
[4] K. Bergmann, H.-C. Nägerl, C. Panda, G. Gabrielse, E. Miloglyadov, M. Quack, G. Seyfang, G. Wichmann, S. Ospelkaus, A. Kuhn *et al.*, J. Phys. B: At., Mol. Opt. Phys. **52**, 202001 (2019).
[5] W. Huang, B. W. Shore, A. Rangelov, and E. Kyoseva, Opt. Commun. **382**, 196 (2017).
[6] D. Møller, J. L. Sørensen, J. B. Thomsen, and M. Drewsen, Phys. Rev. A **76**, 062321 (2007).
[7] K. Kumar, A. Vepsäläinen, S. Danilin, and G. Paraoanu, Nat. Commun. **7**, 10628 (2016).
[8] J. Siewert, T. Brandes, and G. Falci, Opt. Commun. **264**, 435 (2006).
[9] C. Ye, V. Sautenkov, Y. V. Rostovtsev, and M. Scully, Opt. Lett. **28**, 2213 (2003).
[10] U. Hohenester, F. Troiani, E. Molinari, G. Panzarini, and C. Macchiavello, Appl. Phys. Lett. **77**, 1864 (2000).
[11] S. Longhi, Phys. Rev. E **73**, 026607 (2006).
[12] W. Huang, S.-J. Liang, E. Kyoseva, and L. K. Ang, Carbon **127**, 187 (2018).
[13] W. Huang, S. Yin, W. Zhang, K. Wang, Y. Zhang, and J. Han, New J. Phys. **21**, 113004 (2019).
[14] A. A. Rangelov and N. V. Vitanov, Ann. Phys. **327**, 2245 (2012).
[15] N. Sangouard, S. Guérin, L. P. Yatsenko, and T. Halfmann, Phys. Rev. A **70**, 013415 (2004).
[16] B. W. Shore, Acta Phys. Slovaca **63**, 361 (2013).
[17] N. V. Vitanov, Phys. Rev. A **58**, 2295 (1998).
[18] N. V. Vitanov, B. W. Shore, and K. Bergmann, Eur. Phys. J. D **4**, 15 (1998).
[19] B. T. Torosov and N. V. Vitanov, Phys. Rev. A **87**, 043418 (2013).
[20] N. V. Vitanov and S. Stenholm, Phys. Rev. A **60**, 3820 (1999).
[21] W. Huang, S. Yin, B. Zhu, W. Zhang, and C. Guo, Phys. Rev. A **100**, 063430 (2019).
[22] L. D. Contreras-Pulido and R. Aguado, Phys. Rev. B **77**, 155420 (2008).
[23] G. Lindblad, Commun. Math. Phys. **48**, 119 (1976).
[24] V. Gorini, A. Kossakowski, and E. C. G. Sudarshan, J. Math. Phys. **17**, 821 (1976).
[25] I. de Vega and M.-C. Banuls, Phys. Rev. A **92**, 052116 (2015).
[26] E. Mascarenhas and I. de Vega, Phys. Rev. A **96**, 062117 (2017).
[27] C. Guo, I. de Vega, U. Schollwöck, and D. Poletti, Phys. Rev. A **97**, 053610 (2018).
[28] D. M. Fugger, A. Dorda, F. Schwarz, J. von Delft, and E. Arrigoni, New J. Phys. **20**, 013030 (2018).
[29] F. Schwarz, I. Weymann, J. von Delft, and A. Weichselbaum, Phys. Rev. Lett. **121**, 137702 (2018).
[30] X. Xu, J. Thingna, C. Guo, and D. Poletti, Phys. Rev. A **99**, 012106 (2019).
[31] T. Chen, V. Balachandran, C. Guo, and D. Poletti, Phys. Rev. E **102**, 012155 (2020).
[32] I. de Vega, U. Schollwöck, and F. A. Wolf, Phys. Rev. B **92**, 155126 (2015).
[33] R. Bulla, T. A. Costi, and T. Pruschke, Rev. Mod. Phys. **80**, 395 (2008).
[34] M. A. Sillanpää, J. I. Park, and R. W. Simmonds, Nature (London) **449**, 438 (2007).
[35] L. Sárkány, J. Fortágh, and D. Petrosyan, Phys. Rev. A **97**, 032341 (2018).